Hydrol. Earth Syst. Sci. Discuss., 6, 7539–7579, 2009
www.hydrol-earth-syst-sci-discuss.net/6/7539/2009/

Hydrology and Earth System Sciences Discussions

This discussion paper is/has been under review for the journal Hydrology and Earth System Sciences (HESS). Please refer to the corresponding final paper in HESS if available.

Future extreme precipitation assessment in Western Norway – using a linear model approach

G. N. Caroletti[1,2] **and I. Barstad**[1]

[1]Bjerknes Centre for Climate Research, Bergen, Allegata 55, 5007 Bergen, Norway
[2]Geophysical Institute, University of Bergen, Allegata 70, 5007 Bergen, Norway

Received: 24 November 2009 – Accepted: 26 November 2009
– Published: 18 December 2009

Correspondence to: G. N. Caroletti (giulio.caroletti@bjerknes.uib.no)

Published by Copernicus Publications on behalf of the European Geosciences Union.

Abstract

The need for local assessments of precipitation has grown in recent years due to the increase in precipitation extremes and the widespread awareness about findings of the IPCC 2003 Report on climate change. General circulation models, the most commonly used tool for climate predictions, show an increase in precipitation due to an increase in greenhouse gases (Cubash and Meehl, 2001). It is suggested that changes in extreme precipitation are easier to detect and attribute to global warming than changes in mean annual precipitation (Groisman et al., 2005). However, because of their coarse resolution, the global models are not suited to local assessments. Thus, downscaling of data is required.

A Linear Model (Smith and Barstad, 2004) is used to dynamically downscale orographic precipitation over Western Norway from twelve General Circulation Model simulations based on the A1B emissions scenario (IPCC, 2003). An assessment of the changes to future Orographic Precipitation (2046–2065 and 2081–2100 time periods) versus the historical control period (1971–2000) is carried out. Results show an increased number of Orographic Precipitation days and an increased Orographic Precipitation intensity. Extreme precipitation events are up to 20% more intense than the 1971–2000 values. Extremes are defined by the exceedence of the 99%-ile threshold in the time slice. Using station-based observations from the control period, the results from downscaling can be used to generate simulated precipitation histograms at selected stations.

The Linear Model approach also allows for simulated changes in precipitation to be disaggregated according to their causal source: (a) the role of topography and (b) changes to the amount of moisture delivery to the site. The latter can be additionaly separated into moisture content changes due to: (i) temperature; (ii) wind speed; (iii) stability. An analysis of these results suggests a strong role for warming in increasing the intensity of extreme Orographic Precipitation events in the area.

HESSD

6, 7539–7579, 2009

1 Introduction

Precipitation strongly influences human life, and poses great difficulty for the scientist: precipitation results from a chain of different physical processes and varies on spatial and temporal scales. Orographic Precipitation (OP) is of particular interest, as mountain regions occupy about one-fifth of the Earth's surface, are home to one-tenth of the global population and directly affect about half of the world's population (Messerli and Ives, 1997; Becker and Bugmann, 1999). OP is the most important source of fresh water for human communities and for the environment. However, extreme OP events are often the cause of mudslides, avalanches, flash floods, dam breaks, etc. (Roe, 2005).

Precipitation is one of the most difficult meteorological parameters to predict. First and most importantly, precipitation processes are parameterized in even the most complex models. In areas of complex orography, the model resolution needed to properly resolve all important precipitation processes is on the order of kilometers or even less (Smith, 1979).

Although the thermodynamic mechanism of orographic precipitation (e.g., adiabatic cooling and condensation with the uplift of air parcels) is known in its general aspects (Smith, 1979; Roe, 2005), complex topography still makes it difficult for numerical models to accurately reproduce observations (e.g., Bousquet and Smull, 2001; Georgis et al., 2003; Rotunno and Ferretti, 2003; Smith, 2003).

The challenge of matching simulated and observed precipitation is especially acute for General Circulation Models (GCMs). GCM simulations, which provide results on coarse grids of 250–300 km resolution, are not able to account for the observed horizontal variability on smaller scales without great computational investment. The 2007 IPCC Report provides future climate change assessment for precipitation on a global scale through GCMs.

GCM output can be refined with methods that provide local results from global ones, called downscaling. Downscaling can be statistical/empirical (Wilby et al., 1998) or physical/dynamical (Cooley, 2005; Haylock et al., 2006; Schmidli et al., 2007). Statis-

HESSD
6, 7539–7579, 2009

tical downscaling is performed by finding one or more statistical relationships between large scale and finer scale variables (e.g., regression analysis), and then estimating the true local distributions through these relationships. Dynamical downscaling refines large scale information by using physically based models to produce fine-scale information.

Several investigations compared dynamical and statistical downscaling methods for daily precipitation (Wilby et al., 1998; Murphy, 1999; Wilby et al., 2000), showing comparable performance for the two. A comparison between statistical and dynamical methods in regions of complex topography has been carried out in the Alps (Schmidli et al., 2007). Statistical methods have been shown to underestimate interannual variability over the Alps, while the better dynamical models achieve significantly higher skills in winter. Haylock et al. (2006) and Salathé Jr. (2005) suggest the utility of including as many models as possible when developing local climate-change projections.

The most common approach to dynamical downscaling is to use RCMs (Giorgi and Mearns, 1999; Wang et al., 2004). RCMs are high-resolution models run over a limited domain. RCMs typically use relatively low-resolution output from GCMs as boundary conditions. Other approaches involve uniformly high-resolution atmospheric GCMs (Coppola and Giorgi, 2005) and stretched grid models (Deque et al., 1995; Barstad et al., 2008); the latter method simulates the globe with a spatial resolution that varies horizontally to allow for a higher resolution around the area of interest.

The goal of this paper is to use a simpler approach, called the Linear Model (LM from now on; Smith and Barstad, 2004). LM has low computational demands that can be useful for dynamically downscaling simulated precipitation from many climate model runs.

In LM, cloud physics and airflow dynamics are described with a simple set of equations. LM has been successfully used both in idealized (Barstad et al., 2007) and realistic (Crochet et al., 2007) problems predicting orography-induced precipitation: incoming moisture is forced upslope by orography; condensation and drift of cloud-hydrometeors results in precipitation. LM has also been used to simulate extreme

HESSD
6, 7539–7579, 2009

precipitation events (Smith and Barstad, 2004; Barstad et al., 2007). LM has the additional benefit of being able to rigorously separate the simulated cause of changes in OP.

This study focused on Western Norway, a region of steep orography characterized by heavy precipitation on its windward side. The precipitation is the result of strong winds on the upwind side of the mountains, due to the high frequency of extra-tropical cyclones that impact the area (Andersen, 1973, 1975; Barstad, 2002). Precipitation in Western Norway is dominated by forced uplift and not thermally driven convection, so the LM's structural inability to account for convection is not a so severe problem.

The precipitation simulations in this paper will result from the dynamical downscaling of data from 12 IPCC A1B scenario model simulations (IPCC Report, 2007). The A1B scenario is chosen because it represents a moderate emission scenario.

Section 2 describes Smith and Barstad's Linear Model. Section 3 explains the methods used to downscale Western Norway's orographic precipitation and to compare future periods with the control scenario from the recent past. Section 4 explains the downscaled results, with a focus on the change in the number of OP events and the change in magnitude of extreme OP events. Section 5 explains how to apply the results to station data for assessing future precipitation; and by making use of LM's transparency it investigates the reasons for the change in OP extremes. Section 6 provides a summary of results.

2 The linear model

LM makes use of a simple system of equations to describe the advection of condensed water by a mean wind. Smith and Barstad (2004) start by considering a distributed source of condensed water $S(x,y)$ arising from forced ascent (Fig. 1). The source is the sum of a background rate of cloud water generation and local variations created by terrain-forced uplift. Smith and Barstad propose an upslope model enhanced by considering airflow dynamics that provide a source term in Fourier space (variables in

HESSD
6, 7539–7579, 2009

Fourier space are denoted by the simbol "ˆ"):

$$\hat{S}(k,l) = \frac{C_w i\sigma\hat{h}(k,l)}{(1-imH_w)}, \quad (1)$$

assuming saturated conditions (see Table 1 for the explanation of the symbols used).

By following Smith's (2003a) steady-state advection equations describing the vertically integrated cloud water density $q_c(x,y)$ and hydro-meteor density $q_s(x,y)$ and applying simple algebra, an expression for the Fourier transform of the precipitation distribution P is obtained:

$$\hat{P}(k,l) = \frac{\hat{S}(k,l)}{(1+i\sigma\tau_c)(1+i\sigma\tau_f)}, \quad (2)$$

which is dependent on the source $S(x,y)$ and considers time delays (the conversion and fall-out terms τ_c and τ_f).

Combining (1) and (2) gives a "transfer function" relating the Fourier transform of the terrain $\hat{h}$ and the precipitation field $\hat{P}$:

$$\hat{P}(k,l) = \frac{C_w i\sigma\hat{h}(k,l)}{(1-imH_w)(1+i\sigma\tau_c)(1+i\sigma\tau_f)}, \quad (3)$$

whose denominator's factors represent airflow dynamics (first term), cloud delays and advection (second and third terms).

The precipitation distribution is then obtained by an inverse Fourier transform

$$P(x,y) = \iint \hat{P}(k,l)e^{i(kx+ly)}dkdl. \quad (4)$$

The A1B scenario provides daily data for mean horizontal wind (U,V) and mean moist stability frequency N_m. These are constant values for the whole domain, and are updated daily.

In short, the Linear Model describes the effect of orography and mean wind on precipitation, and with some complexity the effect of temperature, humidity, moist stability, conversion and fallout times of hydrometeors.

3 Downscaling GCMs

General Circulation Models (GCMs) have typically too coarse a grid to adequately resolve terrain responsible for orographic precipitation. The LM approach can be used to dynamically downscale GCM data. Variables and parameters used for input to the LM are shown in Table 2.

21 models performed A1B scenario testing, for a total of 41 model runs (Table A1). Not all of them were available due to incomplete data sets or other inconsistencies that could affect the plausibility of our final results. Those which had missing data were dismissed, along with those showing unreasonable predictions for Western Norway temperature (annual average temperature between −40°C and 0°C). Our selection are based on 12 simulations from 10 GCMs (Table 3).

Conversion and fallout times have been set to 1000 s. Typical conversion times are between 200 s and 2000 s (Smith, 2003); longer residence times within clouds result in a delay of the precipitation. The time delays τ=1000 s values are not expected to be exact, but generally summarize the combined effect of many cloud physics processes (Barstad and Smith, 2005), and have been used in LM for studies at the regional scale (Smith, 2006; Crochet et al., 2007). Longer time delays typically result in more precipitation being advected past regions of steep topography, increased precipitation on the lee side of the topography and lower precipitation intensity overall. Conversely, shorter time delays result in more intense rain shifted upwind (Smith and Barstad, 2004; Barstad et al., 2007).

The Linear Model's grid corresponds to the Digital Elevation Model (DEM) GTOPO30 topography grid (US Navy, 2003), and has a resolution of 30″. At a latitude of 60°, this corresponds to an average grid spacing of about 450 m×900 m, sufficient to resolve important scales affecting orographic precipitation.

Our main concern are extreme OP events, so the only days considered are those with a relative humidity above or equal to 85%. Lower relative humidities result in relatively weak to no OP (Barstad et al., 2007). In addition, only days with wind direction between

HESSD
6, 7539–7579, 2009

180° and 300° (westerly winds) were considered, since they are the only ones to give significant OP (Barstad, 2002). Precipitation intensity is calculated in mm/day.

There are several possible ways of defining an extreme event. One alternative is to use the tails of a climatological distribution, through the use of quantiles (Jones, 2000; Cooley, 2005). A second alternative ("peak-over-threshold" method) is to consider as extreme any result exceeding a certain threshold value (Cooley, 2005). An advantage of using the percentile method when performing model-comparison is that it is a relative method that can be used for all model runs and thus provides consistency.

In this paper, the 99th percentile of the distribution is used to define an extreme OP event. Different models use different parameterizations and we do not know a priori which ones are most appropriate for a future situation. Thus, looking at the absolute values could be misleading (Klein Tank and Konnen, 2003). We compare instead the extreme OP intensities of future periods to the control period data within a particular simulation. If simulations from different models agree on a relative increase, then it is more likely to be a consequence of the scenario and not to result from individual model variability.

The model domain is between 57°30′ and 64°20′ N and 4° and 10°40′ E. This includes all of southern Norway. In this area we have selected the 74 grid points nearest to weather stations that were active and measured precipitation during all of the control period 1971–2000. The stations are all located in Western Norway.

4 Results

For illustrative purposes, we first analyze the results for a single station. The chosen station is Bergen-GFI, (lat; lon; height)=(60,38° N; 5,33° E; 22 m a.s.l.).

Figure 3 shows an increase in the relative number of days with orographic precipitation in future periods relative to the control period. All model runs show an increase in OP days in the future periods, although not all agree on whether there will be more days with OP in the first or in the second future period.

HESSD
6, 7539–7579, 2009

In order to evaluate the relative change in the extreme OP intensity from the control period to the future periods, we normalize the absolute 20-years 99th percentile of every model to its own control period 30-years 99th percentile.

The result of this procedure for both future periods is shown in Fig. 4. All models show an increase in the intensity of Orographic Precipitation extremes. The mean ensemble result shows a strong +10% and +16% increase in extreme OP in the 2046–2065 and 2081–2100 intervals, with associated standard deviations of 6% and 11%, respectively.

A time evolution of the ensemble mean 99th percentile of OP is plotted in Fig. 5, with the standard deviation taken into account. Even with the most conservative prediction, we still see an increase in the intensity of the extreme events at the station.

To see if there is a change in pattern as the moist air proceeds into the fjords and mountains, we look at four sections, perpendicular to the coast, two along-fjord (Sognefjord in Sogn-og-Fjordane county and Hardangerfjorden in Hordaland county) and two along-wind cross-sections (one in Hordaland from the city of Bergen to the city of Voss, and the other over the districts of Flora and Gloppen in Sogn-og-Fjordane). The four cross-sections allow us to witness the effect on precipitation of the ascension of the air along its most favorable path (Fig. 6). All show a strong increase in OP extremes in future periods towards the control scenario. There is also an increase in OP extremes from the 2046–2065 period to the 2081–2100 period.

The largest increase in OP intensity happens on the coast, but these stations also exhibit the least significant increases in absolute values, as seen from Table 4 (which shows these only for the first cross-section – Flora-Gloppen). The trend is evident also when grouping all 74 stations on account of their proximity to the coast and elevation in coastal stations, fjord stations, inland/valley stations and mountain stations (Table 5 and Fig. 7). Coastal stations reach almost a 20% increase in the 2081–2100 time period when compared to 1971–2000 extreme OP intensities, while all others present similar result ranging around 9% in 2046–2065 and 14% in 2081–2100.

HESSD
6, 7539–7579, 2009

5 Further applications

5.1 Assessment

Station observations, provided by the Norwegian Meteorological Institute, can be used as a basis for assessing future precipitation changes. We apply the average relative increase in downscaled OP extremes to the station data to generate an estimate of the future absolute intensities of extreme OP.

The 99th percentile of 1971–2000 OP extremes for the Flora-Gloppen section are shown in Table 8. Applying the relative increase for each individual station from the LM (Table 6) results in the 2046–2065 and 2081–2100 estimates shown ("local" method).

For instance, for Gjengedal the 30 years observed 99%-ile of OP is 66.7 mm/day. The model indicates an increase in Gjengedal OP extreme intensities for the 2046–2065 time period of about 10%, with an associated standard deviation of 4%. Thus, the absolute value for 2046–2065 is 73 mm/day, with a standard deviation of 3 mm/day.

An alternative method to retrieve absolute values of future precipitation is to use the relative increase depending on the "geographic setting". In this method, the mean relative increase in extreme OP for all the stations from the group is applied to all stations. This method could provide more reliable data, especially where the precision of our model data is suspect. In situations of high quality output from the downscaled LM, less accurate forecasts could result compared to the "local" method because local variabilities will be smoothed away in the averaging process. Moreover, the mean result will be biased depending on the distribution of available weather stations. The increase and associated standard deviations for the four geographical groups are shown in Table 7. Applying these relative increases to the observed data of the Flora – Gloppen section, we get the results shown in the "geographic setting" columns of Table 8.

We see that there is some difference in the results of the two methods; if we take for instance Grøndalen, for 2046–2065 we see that the value is 94±6 for the first method and 90±5 for the "geographic setting" method. A definitive statement on which method is preferred cannot be provided without a further study of local meteorology.

HESSD
6, 7539–7579, 2009

5.2 Influx analysis

LM can also be used to understand the mechanisms behind downscaled changes in OP extremes.

In order to do this, we calculate the influx of moist air into the region,

$$F = \rho_{S_{\text{ref}}} H_w U \tag{5}$$

where

U is the horizontal wind magnitude;

$\rho_{S_{\text{ref}}} = e_S(T_{\text{ref}})/R_v T_{\text{ref}}$ is the saturation water vapor density at the ground, and

$H_w = -R_v \frac{T_{\text{ref}}^2}{L\gamma}$ is the water vapor scale height.

Furthermore, $e_S(T)$ is the saturation vapor pressure, T_{ref} is the temperature at the ground, $R_v = 461\,\text{J}\,\text{kg}^{-1}\,\text{K}^{-1}$ is the gas constant for vapor, $L = 2{,}5 \times 10^6\,\text{J}\,\text{kg}^{-1}$ is the latent heat and γ is the environmental lapse rate (Smith and Barstad, 2004).

There is a linear relationship between the moist air influx and the precipitation in LM (cf. transfer function (3)); the rest of the OP extreme change is connected to the wind direction at a given station. Figure 8 shows the results of an assessment of the cause of 2046–2065 extreme OP intensities change at the Bergen sample station. Ten simulations out of twelve show a positive sign to the change from moisture influx, and eight out of twelve show a positive sign to the change from wind direction.

The Linear Model offers the possibility to break down the moisture influx to its components. Smith and Barstad (2003) show that the moisture influx (F) depends on density $\rho_S(T)$, $H_w(N,T)$ and wind speed U:

$$F = \rho_{S\,\text{ref}} \times H_w \times U \tag{6}$$

If we write $H = H_w \times \rho_{S\,\text{ref}}$, the increase in influx will be:

$$\frac{dF}{dt} = \frac{d(HU)}{dt} = \frac{dH}{dt}U + H\frac{dU}{dt}. \tag{7}$$

HESSD
6, 7539–7579, 2009

In this way, using the properties of partial differences, we get:

$$\frac{dH}{dt} = \frac{\partial H}{\partial N}\frac{dN}{dt} + \frac{\partial H}{\partial T}\frac{dT}{dt} \tag{8}$$

We can thus rewrite Eq. (6) using Eq. (7):

$$\frac{dF}{dt} = \left(\frac{\partial H}{\partial N}\frac{dN}{dt} + \frac{\partial H}{\partial T}\frac{dT}{dt}\right)U + H\frac{dU}{dt} \tag{9}$$

In Eq. (8) we can compute separately the influence of wind magnitude from the sum of temperature and stability influences on the influx (Fig. 9). A residual, spurious term emerges from the approximations used, but it is shown to be small.

The effect of temperature and stability can now be assessed separately, to see how they contribute to the change in moisture influx. Figure 10 shows that the change in moisture influx is driven primarily by temperature changes in most models.

The combined result of these assessments for Bergen in 2046–2065 (Table 9 and Fig. 11) suggests that temperature is the dominant factor behind increases in OP extreme intensities. All models agree on a temperature increase from the control period to the future period. The dominant role of temperature changes in driving extreme OP increases is our most important and robust result.

Wind speed and direction are important factors to understand a single model, but there is a large model-to-model uncertainty in the importance of both, as evidenced by the high values for standard deviation in Table 9.

Wind direction has an important impact on precipitation. Westerly winds tend to produce more precipitation over the whole region because of the large-scale influence of topography. Local, small-scale topography can partly block moisture influx coming from some directions. For instance, at the Bergen station, LM shows an increase in OP when the wind direction is comprised between 272° and 269°, around 255°, around 231°, and between 217° and 203°.

Because of the big uncertainties in the wind values, including more simulations might give a better picture of the wind's role; however, a possible outcome of adding more

HESSD
6, 7539–7579, 2009

simulations could be that the positive and negative contributions from the models will cancel out and emphasize even more the importance of temperature.

Stability gives only a negligible contribution.

5.3 Discussion

Several studies (Trenberth et al., 2003; Allan and Soden, 2008; Liu et al., 2009) have attributed the widespread increase of heavy precipitation to global warming.

Trenberth et al. (2003) noted that the increase in surface temperature is stronger at higher latitudes. However, the atmospheric general circulation tends to move the moisture from polar regions towards lower latitudes, so there is need for studies addressing whether the increasing moisture would be within reach of extratropical storms that impact the high-latitude regions – a necessary condition for these regions' warming to have an impact on high-latitude precipitation.

Zhang et al. (2007) used observations and GCM simulations to determine whether there was an anthropogenic-warming induced change in precipitation in the 1925–1999 time period. The study, which addressed precipitation over the whole planet, showed an increase in precipitation both in the observations and in the models for Norway, suggesting that these conditions might already have happened during the last century's warming.

Our study addresses Trenberth's concerns in that it shows an increase of OP occurrences at high latitudes, and indicates that temperature change is responsible for about 50% of the future increase in extreme OP values. Temperature changes are more robust than changes to the winds. Due to the uncertainties in wind changes, it is difficult to establish how important they might be in future scenarios. Using wind values from an RCM or downscaling the IPCC wind values could address this problem.

HESSD

6, 7539–7579, 2009

6 Summary

An efficient downscaling method, Smith and Barstad's Linear Model, has been used to physically downscale precipitation from 12 model runs of the IPCC 2007 A1B scenario over Western Norway. The results show an increase in OP occurrence and an increase in the intensity of OP extremes over 74 grid points corresponding to Norwegian weather stations. The increase in intensity is around 10% of the absolute values for the 2046–2065 scenario and around 15% for the 2081–2100 scenario. An an assessment of absolute future changes to extreme OP has been conducted, based on the relative increase of the model results and on weather station observations.

The main reason for the increase of precipitation has been investigated for the Bergen meteorological station. The increase in moist air influx contributes to about two thirds of the increase, while the rest depends on the wind direction. By separating out the factors that contribute to moisture influx, results show that temperature increases are the main cause increased influx, and thus extreme Orographic Precipitation, for all models. Temperature accounts for roughly 50% of the increase in magnitude of the extreme OP events.

The present paper is meant as an introduction to possible uses of analysis connected to LM downscaling and shows methods that can be applied generally to many different model simulations. Downscaling climate scenarios with LM seems to open up interesting possibilities for insight for both climatologists and weather forecasters.

Appendix A

See Tables A1–A4.

Acknowledgements. Many thanks to Anna Fitch and Justin Wettstein for valuable comments on the manuscript.

References

Andersen P.: The distribution of monthly precipitation in Southern Norway in relation to prevailing H. Johansen weather types, Årbok Universitet Bergen, Mat. Naturv. Ser., 1972(1), 1–20, 1973.

Andersen P.: Surface winds in southern Norway in relation to prevailing H. Johansen weather types, Meteor Ann 6(14), 377-399, 1975.

Barstad, I.: Southwesterly flows over southern Norway, Reports in meteorology and oceanography 7, Geofysisk Institutt, UiB, Doctoral Thesis, 2002.

Barstad, I. and Smith, R. B.: Evaluation of an Orographic Precipitation Model, J. Hydrometeorol., 6, 85–99, 2005.

Barstad, I., Grabowski, W. W., and Smolarkiewicz, P. K.: Characteristics of large-scale orographic precipitation, J. Hydrol., 340, 78–90, 2007.

Barstad, I., Sorteberg, A., Flatoy, F., and Déqué, M.: Precipitation, temperature and wind in Norway: dynamical downscaling of ERA40, Clim. Dynam., 33, 769–776, 2008.

Becker, M. and Bugmann, H.: Global Change and Mountain Regions – The Mountain Research Initiative, Global Terrestrial Observing System, Report n. 28, 1999.

Bousquet, O. and Smull, B. F.: Comparative study of two orographic precipitation events exhibiting significant upstream blocking during MAP, in Extended abstracts from the MAP meeting 2001, MAP Newsletter 15, 2001.

Christensen, J. H., Hewitson, B., Busuioc, A., Chen, A., Gao, X., Held, I., Jones, R., Kolli, R. K., Kwon, W.-T., Laprise, R., Magaña Rueda, V., Mearns., L., Menéndez, C. G., Räisänen, J., Rinke, A., Sarr, A., and Whetton, P.: Regional Climate Projections. In: Climate Change 2007: The Physical Science Basis. Contribution of Working Group I to the Fourth Assessment Report of the Intergovernmental Panel on Climate Change, edited by: Solomon, S., Qin, D., Manning, M., Chen, Z., Marquis, M., Averyt, K. B., Tignor, M., and Miller, H. L., Cambridge University Press, Cambridge, United Kingdom and New York, NY, USA, 2007.

Cooley, D. S.: Statistical Analysis of Extremes Motivated by Weather and Climate Studies:

Applied and Theoretical Advances, Doctoral Thesis, University of Colorado at Boulder, Department of Applied Mathematics, 1–122, 2005.
Coppola, E. and Giorgi, F.: Climate change in tropical regions from high resolution time slice AGCM experiments, Q. J. Roy. Meteor. Soc., 131B, 3123–3146, 2005.
Crochet, P., Johannesson, T., Jonsson, T., Sigurdsson, O., Bjornsson, H., Palsson, F., and Barstad I.: Estimating the Spatial Distribution of Precipitation in Iceland Using a Linear Model of Orographic Precipitation, J. Hydrometeorol., 8, 1285–1306, 2007.
Déqué, M. and Piedelievre, J. P.: High-Resolution climate simulation over Europe, Clim. Dynam., 11, 321–339, 1995.
Georgis, J.-F., Roux, F., Chong, M., and Pradier, S.: Triple-Doppler radar analysis of the heavy rain event observed in the Lago Maggiore region during MAP IOP 2b, Q. J. Roy. Meteor. Soc., 129, 495–522, 2003.
Giorgi, F. and Mearns, L. O.: Introduction to special section: Regional climate modeling revisited, J. Geophys. Res., 104, 6335–6352, 1999.
Groisman, P., Knight, R. W., Easterling, D. R., Karl, T. K., Hegerl, G., and Razuvaev, V. N.: Trends in Intense Precipitation in the Climate Record, J. Climate, 18, 1326–1350, 2005.
Haylock, M. R., Cawley, G. C., Harpham, C., Wilby, R. L., and Goodess, C. M.: Downscaling Heavy Precipitation over the United Kingdom: A comparison of dynamical and statistical methods and their future scenarios, Int. J. Climatol., 26, 1397–1415, 2006.
Jones, C.: Occurrence of Extreme Precipitation Events in California and Relationships with the Madden-Julian Oscillation, J. Climate, 13, 3576–3587, 2000.
Klein Tank, A. M. G. and Konnen, G. P.: Trends in Indices of Daily Temperature and Precipitation Extremes in Europe, 1946–1999, J. Climate, 16, 3665–3680, 2003.
Liu, S. C., Fu, C., Shiu, C.-J., Chen, J.-P. and Wu, F.: Temperature dependence of global precipitation extremes, Geophys. Res. Lett., 36, L17702, doi:10.1029/2009GL040218, 2009.
Messerli, B. and Ives, J. D.(Eds.): Mountains of the World: A Global Priority, Parthenon Pub. Group, New York, USA, 495 pp., 1997.
Murphy, J.: An evaluation of statistical and dynamical techniques for downscaling local climate, J. Climate, 12(8), 2256–2284.1999.
Roe, G.: Orographic Precipitation, Annu. Rev. Earth Pl. Sc., 33, 645–671, 2005.
Rotunno, R. and Ferretti, R.: Orographic effects on rainfall in MAP cases IOP 2b and IOP 8, Q. J. Roy. Meteor. Soc., 129, 373–390, 2003.
Salathé Jr., E. P.: Downscaling simulations of future global climate with application to hydrologic

modelling, Int. J. Climatol., 25, 419–436, 2005.
Schmidli, J., Goodess, C. M., Frei, C., Haylock, M. R., Hundecha, Y., Ribalaygua, J., and Schmith, T.: Statistical and dynamical downscaling of precipitation: An evaluation and comparison of scenarios for the European Alps, J. Geophys. Res., 112, D04105, 1–20, 2007.
Smith, R. B.: The influence of mountains on the atmosphere, Adv. Geophys., 21, 87–230, 1979.
Smith, R. B.: A linear upslope-time-delay model for orographic precipitation, J. Hydrol., 282, 2–9, 2003.
Smith, R. B.: Progress on the theory of orographic precipitation, Geological Society of America, Special Paper, 398, 1–16, 2006.
Smith, R. B. and Barstad, I.: A linear theory of orographic precipitation, J. Atmos. Sci., 61, 1377–1391, 2004.
Trenberth, K. E., Dai, A., Rasmussen, R. M., and Parsons, D. B.: The changing character of precipitation, B. Am. Meteorol. Soc., 84, 1205–1217, 2003.
Wang, Y., Leung, L. R., McGregor, J. L., Lee, D. K., Wang, W. C., Ding, Y., and Kimura, F.: Regional climate modeling: progress, challenges and prospects, J. Meteorol. Soc. Jpn., 82(6), 1599–1628, 2004.
Wilby, R. L., Wigley, T. M. L., Conway, D., Jones, P. D., Hewitson, B. C., Main, J., and Wilks, D. S.: Statistical downscaling of general circulation model output: A comparison of methods, Water Resour. Res., 34, 2995–3008, 1998.
Wilby, R. L. and Wigley, T. M. L.: Downscaling general circulation model output: A reappraisal of methods and limitations. In Climate Prediction and Agriculture, edited by: Sivakumar, M. V. K., Proceedings of the START/WMO International Workshop, 27–29 September 1999, Geneva, International START Secretariat, Washington, DC, 39–68, 2000.
Zhang, X., Zwiers, F. W., Hegerl, G. C., Lambert, F. H., Gillett, N. P., Solomon, S., Stott, P. A., and Nozawa, T.: Detection of human influence on twentieth-century precipitation trends, Nature, 448, 461–465.

Table 1. Some symbols used in the model.

Symbol	Physical property	Typical values
(k,l)	Components of the horizontal wavenumber vector	
C_w	Thermodynamics uplift sensitivity factor	0.001 to 0.02 kg m^{-3}
$\sigma = Uk + Vl$	Intrinsic frequency	0.01 to 0.0001 s^{-1}
$h(x,y)$	Height of terrain	
$m(k,l)$	Vertical wavenumber	0.01 to 0.0001 m^{-1}
H_w	Depth of moist layer (water vapor scale height)	1 to 5 km

HESSD
6, 7539–7579, 2009

Table 2. Model inputs.

Input Variable	Symbol	Data Source
Wind	U	GCM data
Temperature	T	GCM data
Moist static stability	Nm	GCM data
Humidity	q	GCM data
Relative humidity	RH	GCM data
Terrain	h	DEM topography
Conversion time	τ_c	User defined as 1000 s
Fallout time	τ_f	User defined as 1000 s
Background precipitation	–	User defined as 0 mm h^{-1}

HESSD
6, 7539–7579, 2009

Table 3. Downscaled IPCC model runs.

Model Number	Model Run Name	Model Number	Model Run Name
1	gfdl_cm2_1	7	cnrm_cm3_1
2	gfdl_cm2_0	8	miroc_hires
3	mri_cgcm2_3_2a_1	9	miroc_medres
4	cccma_cgcm3_1_t47 run 1	10	mpi_echam5
5	cccma_cgcm3_1_t47 run 2	11	cccma_cgcm3_1_t63
6	cccma_cgcm3_1_t47 run 3	12	bccr_bcm2_0

HESSD
6, 7539–7579, 2009

Table 4. Mean of extreme OP intensities for twelve model-runs for Flora and Gloppen districts stations, expressed in absolute values (mm/day), including standard deviation.

	FLORA-GLOPPEN				99%-ile (mm/day)	
Station name	1971–2000	std	2046–2065	std	2081–2100	std
Ytterøyane Fyr	15,6	**2,2**	17,9	**2,5**	18,7	**2,6**
Kinn	20	**2,7**	22,8	**3,1**	23,9	**3,2**
Eikfjord	88,9	**11,0**	99,4	**12,8**	103,4	**12,9**
Grøndalen	120,3	**17,6**	135,0	**22,7**	139,5	**21,0**
Gjengedal	83,6	**17,2**	92,0	**18,8**	97,5	**17,9**

HESSD
6, 7539–7579, 2009

Table 5. Changes in extreme OP intensities by geographic setting, relative to the 1971–2000 control period. "Mountain" stations are inland stations located above 400 m a.s.l.

Relative mean extreme intensities by geographic setting	1971–2000	2046–2065	2081–2100
Coast (7 stations)	100%	113%	119%
Fjord (29 stations)	100%	110%	114%
Inland (22 stations)	100%	109%	114%
Mountain (16 stations)	100%	109%	114%
Mean of all 74 stations	100%	110%	115%

HESSD
6, 7539–7579, 2009

Table 6. Flora-Gloppen section. Relative increase of extreme OP intensity to the control scenario as a mean intensity of 12 LM-downscaled model runs.

STATION	2046–2065 % increase	2081–2100 % increase
Ytterøyane Fyr	14±4	20±8
Kinn	14±4	20±8
Eikfjord	12±4	16±6
Grøndalen	12±7	16±7
Gjengedal	10±4	17±7

HESSD
6, 7539–7579, 2009

Table 7. Twelve-model runs 99%-ile of orographic precipitation, expressed as an increase relative to the 1971–2000 control period, for all stations divided into four groups depending on their geographic setting, with associated standard deviation.

99%-ILE OP	2046–2065 % increase	2081–2100 % increase
Coast	13±4	19±7
Fjord	10±7	14±8
Inland	9±6	14±7
Mountain	9±7	14±8

HESSD
6, 7539–7579, 2009

Table 8. Flora-Gloppen section. Extreme OP intensity of station data from Norwegian Meteorological Institute and assessment of future orographic precipitation extremes, obtained via local increase method and geographic setting increase method.

ASSESSING OP EXTREMES (mm/day)		WITH "LOCAL" STATIONS INCREASE		WITH "GEOGRAPHIC SETTING" INCREASE	
Station	1971–2000 observed	2046–2065 assessment	2081–2100 assessment	2046–2065 assessment	2081–2100 assessment
Ytterøyane Fyr	26,9	31±1	32±2	30±2	31±2
Kinn	39,0	44±2	47±3	44±2	46±3
Eikfjord	66,7	75±3	77±4	72±3	75±5
Grøndalen	84,0	94±6	97±6	90±5	95±6
Gjengedal	66,1	73±3	77±5	71±4	74±5

HESSD
6, 7539–7579, 2009

Table 9. Percent contributions for the increase in extremes by the factors affecting precipitation.

Factor	Contribution to OP extremes increase	Standard deviation
Temperature	46%	±25%
Wind direction	33%	±66%
Wind magnitude	16%	±61%
Stability	4%	±4%
Residual	1%	±4%

HESSD
6, 7539–7579, 2009

Table A1. A1B scenario and model runs. Modified from Ersdal, Geophysical Institute, UiB, internal report.

Model	Runs	Problem	Status
bccr_bcm2_0	Run 1	–	OK
cccma_cgcm3_1_t47	Runs 1–3	–	OK
cccma_cgcm3_1_t63	Run 1	–	OK
cnrm_cm3	Run 1	–	OK
csiro_mk3_0	Run 1	Starts 30.12.2045	–
csiro_mk3_5	Run 1	Starts 30.12.2045	–
gfdl_cm2_0	Run 1	–	OK
gfdl_cm2_1	Run 1	–	OK
giss_aom	Run 1	Missing data	–
giss_model_e_r	Run 1	–	To do
iap_fgoals1_0_g	Runs 1–3	Unreasonable values	–
ingv_echam4	Run 1	360 days a year	–
inmcm3_0		Missing year info	–
ipsl_cm4		360 days a year	–
miroc3_2_hires	Run 1	–	OK
miroc3_2_medres	Run 1	–	OK
miub_echo_g	Run 1	360 days a year	–
mpi_echam5	Run 2	–	OK
mri_cgcm2_3_2a	Run 1	–	OK
ncar_ccsm3_0	Runs 2–8	Missing variables.	–
ncar_pcm1	Runs 1–2	Missing variables.	–

Modified from Ersdal, 2007, UiB internal report.

HESSD
6, 7539–7579, 2009

Table A2. Ratio of days with orographic precipitation to total number of days for three time slices, 12 model runs, Bergen-GFI station.

	BERGEN-GFI	% of OP days				
	Model name	1971–2000	2046–2065	*increase*[a]	2081–2100	*increase*[a]
1	gfdl_cm2_1	100%	111%	**+11%**	124%	**+24%**
2	gfdl_cm2_0	100%	110%	**+10%**	118%	**+18%**
3	mri_cgcm2_3_2a	100%	110%	**+10%**	114%	**+14%**
4	cccma_cgcm3_1_t47 run 1	100%	111%	**+11%**	107%	**+7%**
5	cccma_cgcm3_1_t47 run 2	100%	103%	**+3%**	114%	**+14%**
6	cccma_cgcm3_1_t47 run 3	100%	111%	**+11%**	103%	**+3%**
7	cnrm_cm3	100%	113%	**+13%**	126%	**+26%**
8	miroc3_2_hires	100%	109%	**+9%**	114%	**+14%**
9	miroc3_2_medres	100%	107%	**+7%**	106%	**+6%**
10	mpi_echam5	100%	104%	**+4%**	111%	**+11%**
11	cccma_t63	100%	111%	**+11%**	109%	**+9%**
12	bccr_bcm2_0	100%	127%	**+27%**	142%	**+42%**
	ENSAMBLE MEAN	100%	111%	**+11%**	116%	**+16%**
	Standard deviation			**6%**		**11%**

[a]Increase is in both cases evaluated in respect to the 1971–2000 control period.

HESSD
6, 7539–7579, 2009

Table A3. 99%-ile of orographic precipitation for 12 model runs, Bergen Florida station. The first and last year of the scenarios have a three years forward running mean, while the second and next-to-last have a four years forward running mean.

	BERGEN FLORIDA	99%-ile				
	Model name	1971–2000	2046–2065	*increase*[a]	2081–2100	*increase*[a]
1	gfdl_cm2_1	51,0	56,6	**+11%**	57,5	**+13%**
2	gfdl_cm2_0	50,4	55,4	**+10%**	58,8	**+17%**
3	mri_cgcm2_3_2a	48,6	54,2	**+11%**	56,7	**+17%**
4	cccma_cgcm3_1_t47 run 1	56,0	59,6	**+6%**	62,2	**+11%**
5	cccma_cgcm3_1_t47 run 2	56,1	60,6	**+8%**	60,8	**+8%**
6	cccma_cgcm3_1_t47 run 3	55,7	62,3	**+12%**	62,8	**+13%**
7	cnrm_cm3	46,8	49,7	**+6%**	51,9	**+11%**
8	miroc3_2_hires	62,1	73,0	**+17%**	76,7	**+23%**
9	miroc3_2_medres	54,3	63,7	**+17%**	67,6	**+24%**
10	mpi_echam5	54,2	61,2	**+12%**	62,7	**+16%**
11	cccma_t63	56,9	63,3	**+11%**	65,5	**+15%**
12	bccr_bcm2_0	43,2	48,1	**+11%**	49,2	**+14%**
	ENSAMBLE MEAN	52,9	59,0	**+11%**	61,0	**+15%**
	Standard deviation	5,2	6,8	**4%**	7,2	**5%**

[a]Increase in both cases refers to the 1971–2000 period.

HESSD
6, 7539–7579, 2009

Table A4. Mean values for wind magnitude, stability and temperature during extreme OP events, comparing 1971–2000 means with 2046–2065 for every model run and showing the 12-model runs average.

BERGEN	1971–2000			2046–2065		
Model Run	Temperature	Wind magnitude	Stability	Temperature	Wind magnitude	Stability
1	285,34	12,04	0,0067	286,51	12,5	0,0070
2	285,07	10,7	0,0067	285,93	12,06	0,0069
3	284,77	12,84	0,0063	285,82	13,1	0,0069
4	286,21	14,09	0,0074	287,21	13,04	0,0073
5	286,09	12,87	0,0072	287,31	13,26	0,0073
6	285,74	13,64	0,0075	287,14	14,07	0,0077
7	285,56	9,4	0,0059	286,08	10,27	0,0065
8	288,56	10,81	0,0061	291,34	10,84	0,0061
9	285,91	14,53	0,0073	288,71	13,29	0,0075
10	286,63	13,58	0,0064	287,9	14,62	0,0068
11	285,66	15,83	0,0078	287,25	17,41	0,0080
12	284,6	11,73	0,0056	285,57	12,18	0,0058
MEAN	**285,9**	**12,7**	**0,0067**	**287,2**	**13,1**	**0,0070**

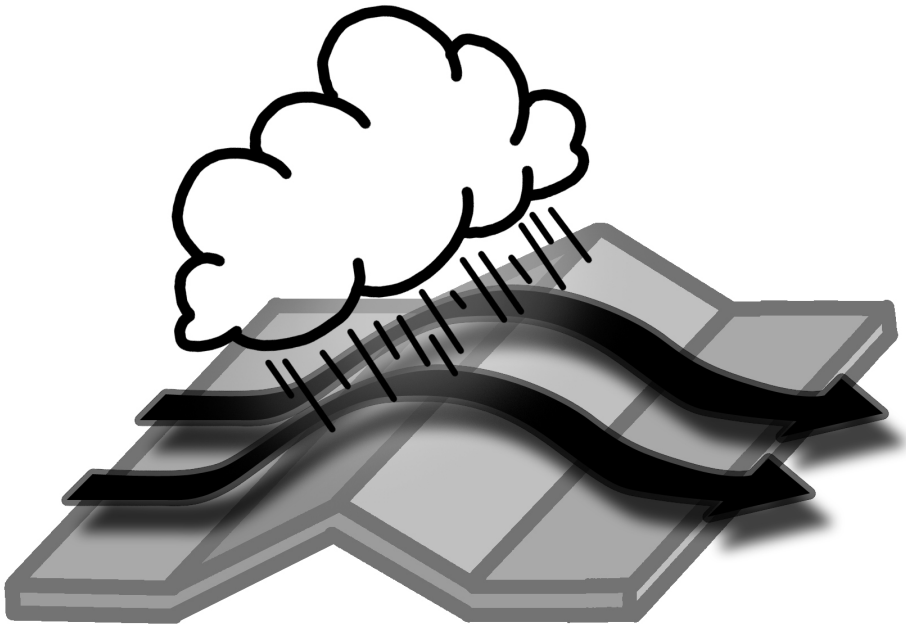

Fig. 1. A schematic illustration of orographic precipitation as the result of stable upslope ascent. Illustration by Marco Caradonna, 2009, based on a figure from Roe, 2005.

HESSD

6, 7539–7579, 2009

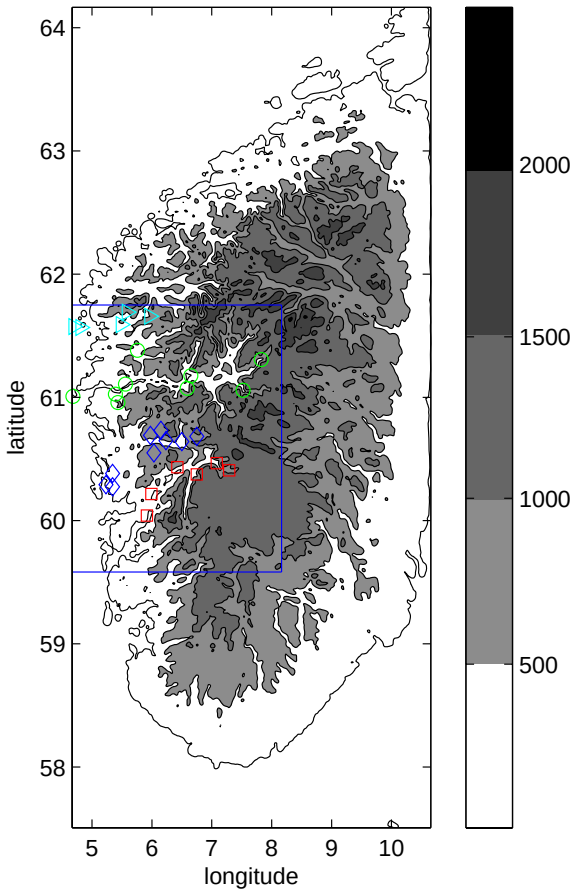

Fig. 2. The domain area. Note the smoothing of mountains near the boundaries. The points show the location of the meteorological stations used for the cross-sections in Sect. 4 (see also Fig. 6).

HESSD

6, 7539–7579, 2009

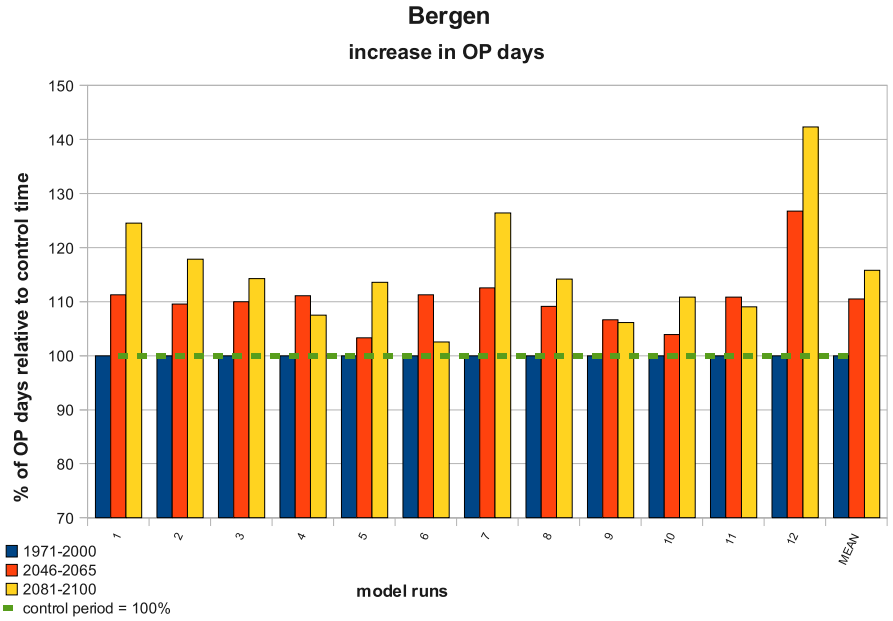

Fig. 3. Percent of OP days out of total number of days for scenario periods, compared to OP days of control period. The last column on the right shows the mean of the 12 model-runs. The model numbers refer to Table 3.

HESSD
6, 7539–7579, 2009

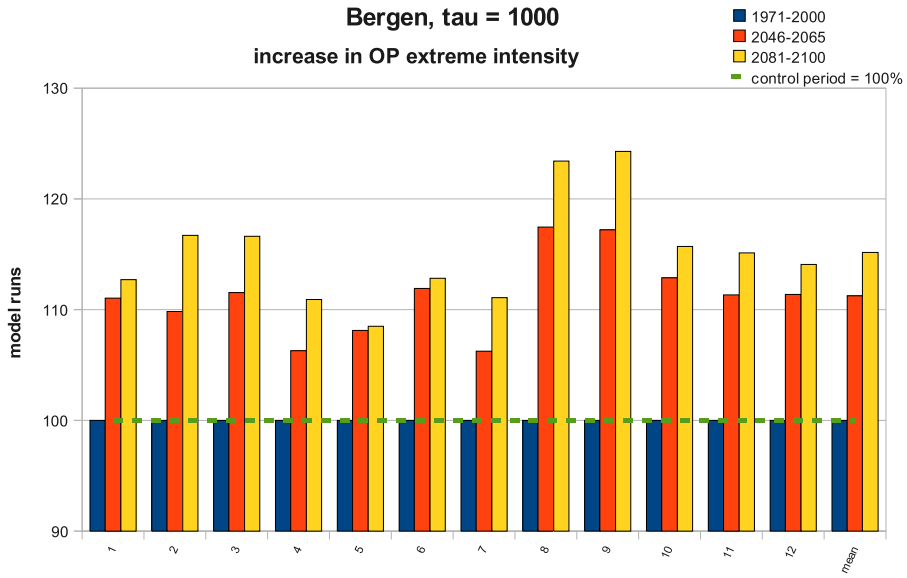

Fig. 4. Percent of extreme intensity of OP from control period to future periods.

HESSD
6, 7539–7579, 2009

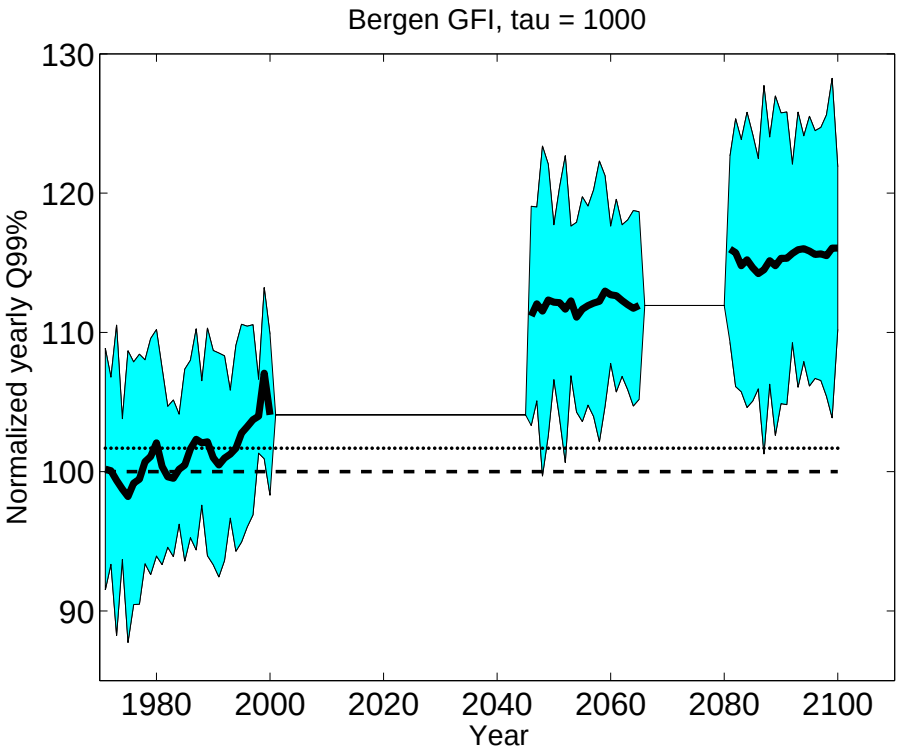

Fig. 5. Yearly mean extremes with 12-model yearly standard deviation shaded in cyan. The upper dotted line shows the mean of the yearly extreme OP intensities; the lower dashed line shows the 1971–2000 30 years averaged mean extreme OP. The time evolution of the ensemble mean 99th percentile of OP is performed by calculating the yearly 99%-ile for every year and every model of our study, and then by performing a 5-year running mean. By using an ensemble mean, the trend in extreme event intensity is not hidden by the annual variability in individual model runs.

HESSD
6, 7539–7579, 2009

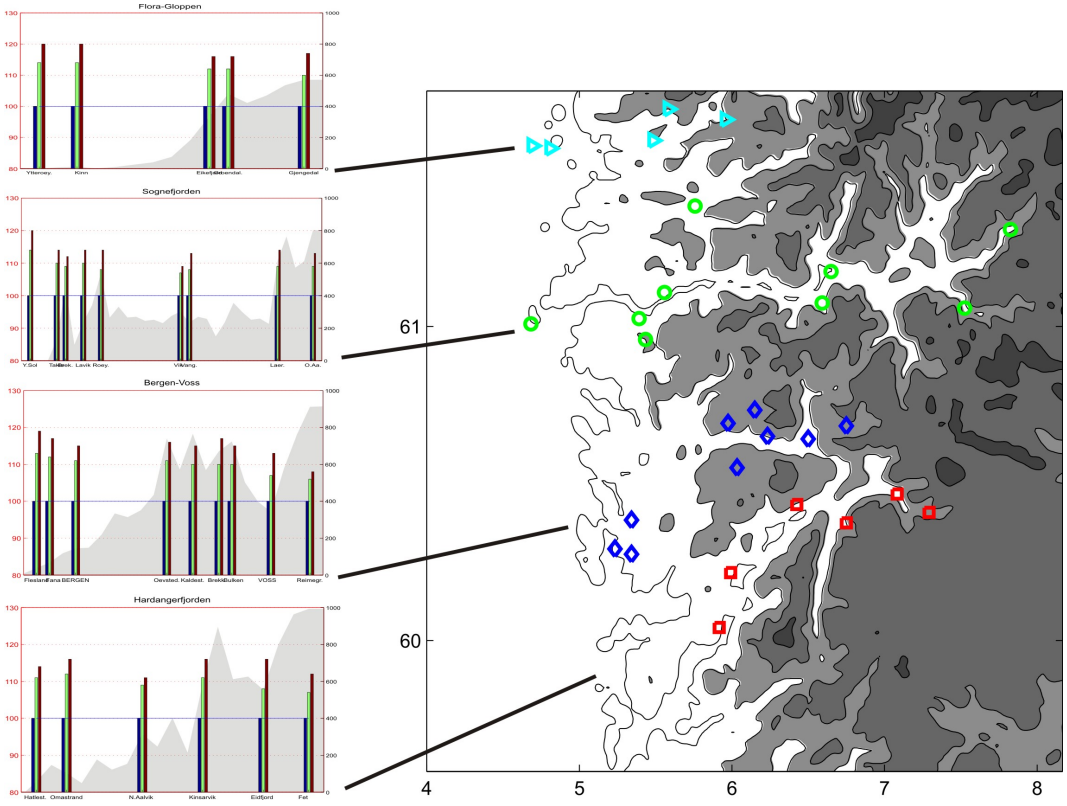

Fig. 6. Twelve-models relative increase in extreme OP for four sections of Norway's western coast. The stations' locations are shown on the map on the right (see Fig. 2 for the position of this region in the domain's area). The gray shading shows the height a.s.l. along the sections.

HESSD
6, 7539–7579, 2009

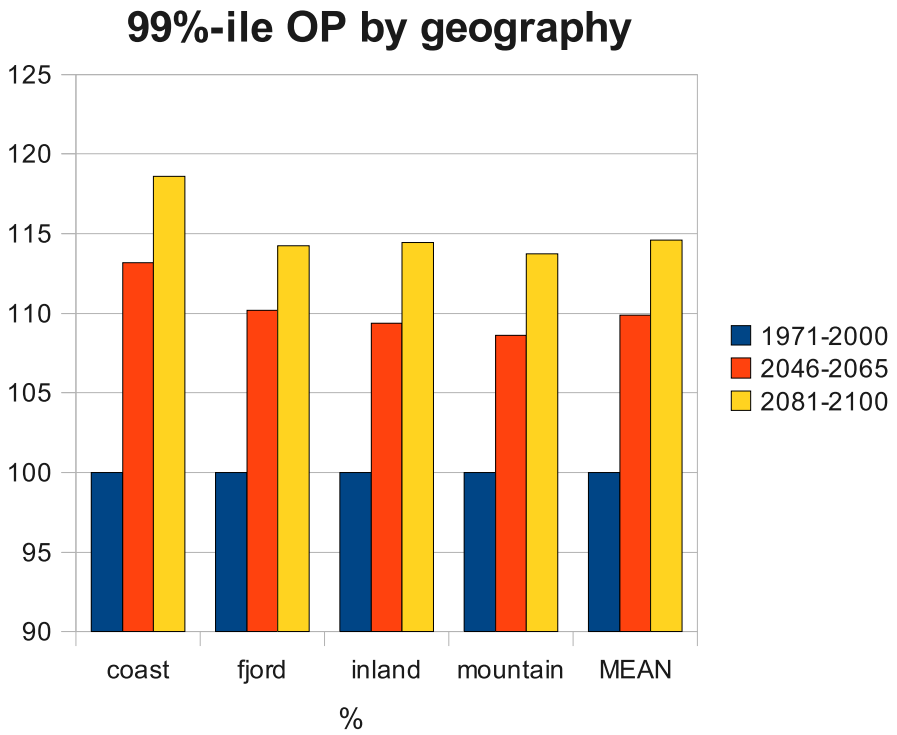

Fig. 7. 99%-ile of orographic precipitation, for twelve model runs, expressed as an increase relative to the 1971–2000 control period, for all stations divided into four groups depending on their geographical location.

HESSD
6, 7539–7579, 2009

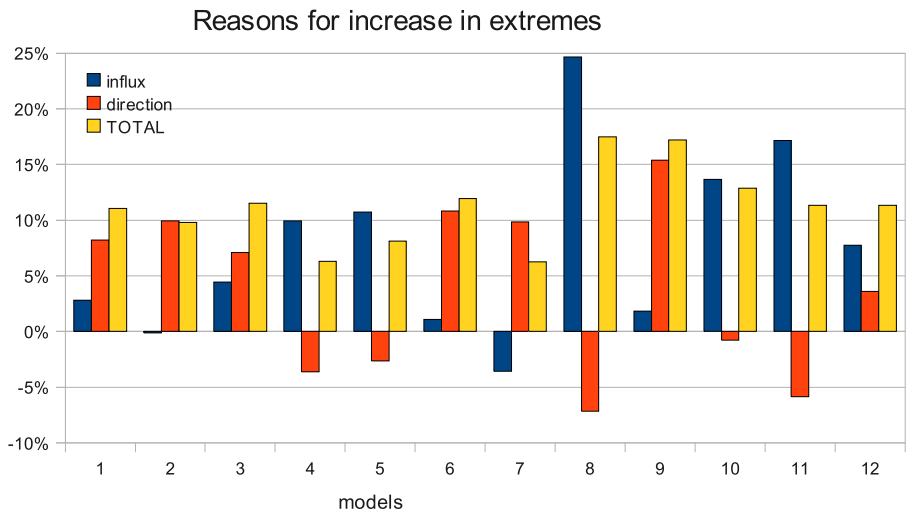

Fig. 8. Reasons for the increase in extremes of 2046–2065 OP days for the Bergen meteorological station compared to 1971–2000 OP days. The total increase is the sum of the influx part and the direction part.

HESSD

6, 7539–7579, 2009

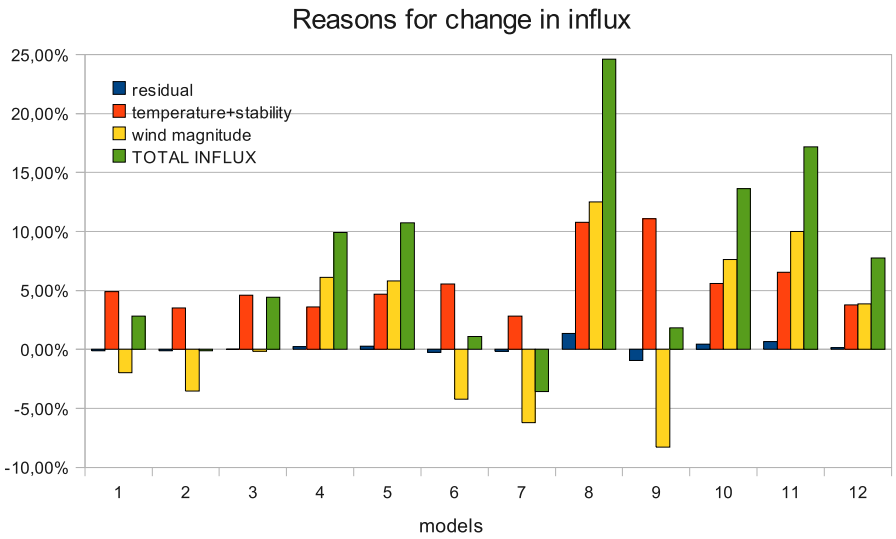

Fig. 9. Reasons for the change in influx of 2046–2065 extreme OP days for the Bergen meteorological station compared to 1971–2000 extreme OP days.

HESSD
6, 7539–7579, 2009

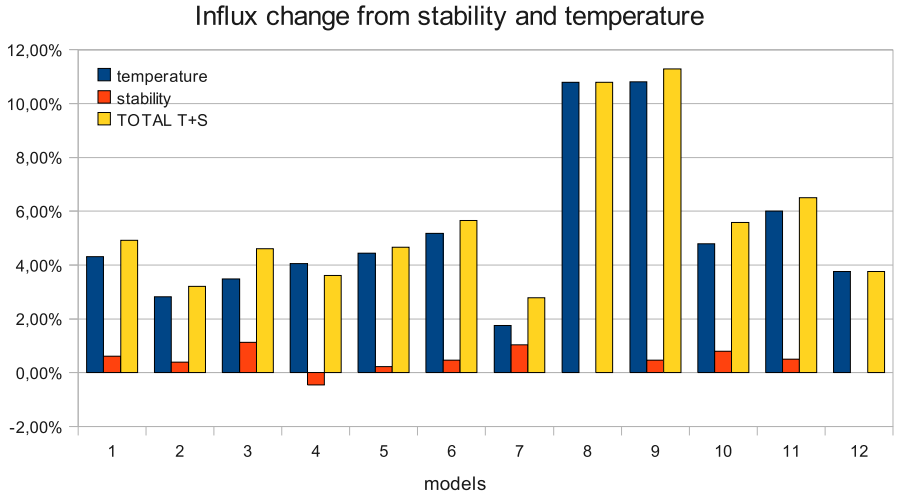

Fig. 10. Contribution of stability and temperature to influx change in extreme OP events. Bergen station, 2046–2065 time period compared to 1971–2000 time period.

HESSD
6, 7539–7579, 2009

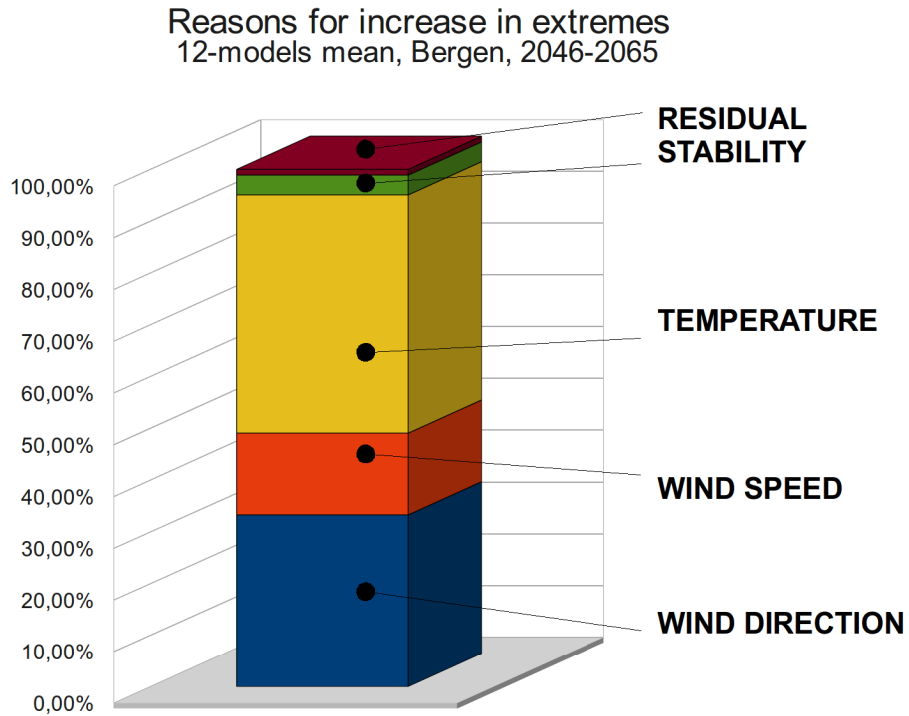

Fig. 11. Percent contributions for the increase in extremes by the factors affecting precipitation. The corresponding numbers and associated spread are shown in Table 9.

HESSD
6, 7539–7579, 2009